Superconductor Science and Technology

PAPER

BOX: an efficient benchmark facility for the study and mitigation of interface-induced training in accelerator type high-field superconducting magnets

To cite this article: Michael Daly *et al* 2021 *Supercond. Sci. Technol.* **34** 115008

IOP Publishing Superconductor Science and Technology
Supercond. Sci. Technol. **34** (2021) 115008 (9pp) https://doi.org/10.1088/1361-6668/ac2002

BOX: an efficient benchmark facility for the study and mitigation of interface-induced training in accelerator type high-field superconducting magnets

Michael Daly[1,*], Bernard Auchmann[1], Christoph Hug[1], Serguei Sidorov[1], Simon Otten[2], Anna Kario[2], Marc Dhallé[2] and Herman Ten Kate[2]

[1] Paul Scherrer Institute, Villigen, Switzerland
[2] Faculty of Science and Technology, University of Twente, Enschede, The Netherlands

E-mail: michael.daly@psi.ch

Received 27 April 2021, revised 30 July 2021
Accepted for publication 23 August 2021
Published 28 September 2021

Abstract

For 30 years, training and unpredictable degradation in accelerator type high-field Nb_3Sn magnets have seriously hampered Nb_3Sn application. Training and deterioration have to be solved or at least better controlled. The global picture shows that most of the R&D and short model magnets start to train at some 40%–70% of the critical current and then creep up to almost the critical current within some 10–50 training steps. A typical class of failures leading to quenches is largely characterized by cracking and debonding at the interfaces between cable and glass-resin insulation, as well as between insulation and coil former. The study of training by means of testing demonstrator coils is rather expensive and time consuming. However, advances in magnet design and fabrication can also be assessed and benchmarked using BOX, the bonding experiment presented here, that produces maximum uniaxial Lorentz forces at some 7.5 T in a controlled experiment performed in 11 T solenoid facility at the University of Twente. BOX samples use only one meter of Nb_3Sn cable inserted in a three-wave meandering slot in a flat metallic sample holder, reproducing magnet-relevant interactions between cable, insulation, impregnated materials and coil former. The meander shape exposes seven straight cable sections to a transverse magnetic field, thereby generating a representative level of shear stress at the interfaces. In this way, characteristic training curves of magnets can be mimicked and solutions studied. We aim to demonstrate with various samples failure mechanisms of high-field Nb_3Sn magnets without the need to manufacture complete magnets. BOX may thus be expected to allow for quick and affordable testing of novel insulations, impregnation materials, coatings and interfaces for Nb_3Sn magnets achieved by investigating various resins, fillers and more.

Keywords: debonding experiment, Nb&lt, sub&gt, 3&lt, /sub&gt, Sn, canted cosine theta, magnet training, Rutherford cable, impregnation, quench

(Some figures may appear in colour only in the online journal)

* Author to whom any correspondence should be addressed.

1. Introduction

High-field Nb_3Sn accelerator type magnets are frequently subject to lengthy magnet training [1]. In part, this is due to the electrical insulator and encapsulating epoxy resin materials and their interaction with the cable and coil structural elements [2, 3]. Invariably, the epoxy resin also functions as a glue that binds the cable–glass–epoxy composite to structural coil components, such as wedges, spacers, central poles, or winding formers. These are fundamental components of stress-management coil concepts, which aim to intercept Lorentz forces within the coil. This is for example the case in canted cosine theta (CCT) magnets, where each individual turn is wound into a helical channel in the winding former [4–7] and similarly in the winding blocks of stress-managed cosine theta (SM-CT) magnets, where turns are positioned in wider axial slots of a former [8, 9].

All interfaces in and between the composite winding packs and structural elements have in common that they can crack or debond when excessive shear or tensile stress is applied. Examples of debonding from coil components have been found in R&D magnets of the high-luminosity LHC project [10–12]. Furthermore, debonding from the CCT channel walls is assumed to be a major impediment also to this type of magnets' performance [13, 14]. Similarly, bonding issues in SM-CT coils are potential risks to be mitigated [8]. Figure 1 provides a characteristic example of observed cracks in a CCT magnet running along the interface with the channel wall as well as further cracking on the surface resin above the conductor.

Debonding involves a local release of energy which can cause a magnet to quench [15, 16]. Even worse, unstable interfaces may allow for stick-slip motion at the interface [17], or introduce cracks that propagate within the epoxy resin and the glass-resin composite itself, all of which contribute to an overall deterioration of magnet performance. It remains to be seen whether unreliable interfaces also play a significant role in the thermal-cycling related performance issues that have plagued several high-field Nb_3Sn magnets in the recent past.

In general, bonding strength in Nb_3Sn coils is affected by a number of factors, among which: (a) surface topology and roughness of the interface [18]; (b) cleanliness of the interface [19]; (c) thermal-contraction mismatch between the resin and the structural element [20]; and (d) the fracture toughness of the epoxy resin [21–23]. Similarly, the likelihood of interface-induced cracks is influenced by the above factors, as well as by local stress concentrations.

Numerous approaches, some complementary and some mutually exclusive, have been proposed to mitigate interface problems. These can be summarized as: (a) replacing all bonded interfaces by sliding interfaces; (b) replacing the epoxy system with brittle substances like paraffin or beeswax that releases less energy upon fracture [24]; (c) increasing the epoxy's fracture toughness [21]; (d) using filled epoxy systems in order to reduce differential thermal contraction; (e) removing reaction residues and dirt from interfaces [19, 25]; and (f) increasing heat capacity [26]. Given the typical time- and cost-considerations of superconducting magnet R&D, only a limited number of ideas can normally be implemented in R&D magnets, and more exotic approaches are thus hardly ever tested.

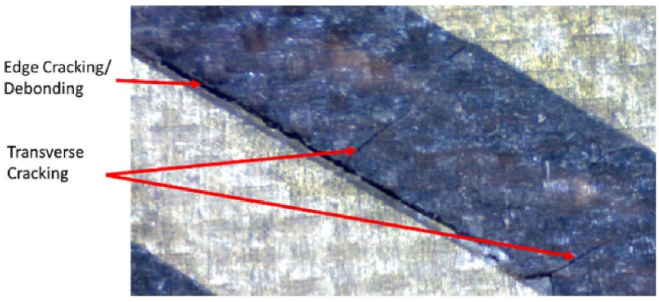

Figure 1. Example of damage in a CCT-5 Nb_3Sn coil. Debonding is observed along the epoxy resin impregnated conductor (dark/blueish material) and the aluminium-bronze former (gold/metallic material). Cracking is also present at the surface of the resin-impregnated conductor composite (Courtesy of Lawrence Berkeley National Laboratory (LBNL) [14]).

In this paper we propose and demonstrate a new method for studying performance limitations in superconducting accelerator type of magnets, however, the results may also be relevant for other magnets. We introduce a new subscale test facility called the BOX (bonding experiment). The facility comprises a representative cable sample, see figure 2, inserted in the bore of a solenoid that provides a background magnetic field at 4.2 K. Remarkably, slightly more than a meter of cable is required, keeping the material cost of the sample low with respect to the budget for testing. Furthermore, the overall cost and turn-around time are more than an order of magnitude smaller compared to the testing of short R&D magnets for assessing conductors, electrical insulation and resins. In this way, the BOX facility opens up the possibility to do low-risk wide-ranging and innovative research for testing bonding materials and to study interface issues for general purposes, but also to find optimal custom-made solutions for specific magnets.

2. Sample and experiment design

2.1. BOX design

The BOX sample as shown in figure 2 comprises three main parts: the main body with the channel containing the cable, the cable itself, and the faceplate that prevents the cable from moving out of the channel. The channel is sufficiently deep and wide to allow movement of the cable during the heat treatment and to avoid compression of the cable during fabrication and when closing the faceplate once fully impregnated. Within the context of for example a CCT magnet, the faceplate is replaced by an outer layer or a shell. Furthermore, the faceplate follows all steps of fabrication and can also be removed for non-destructive observations of the meandering conductor

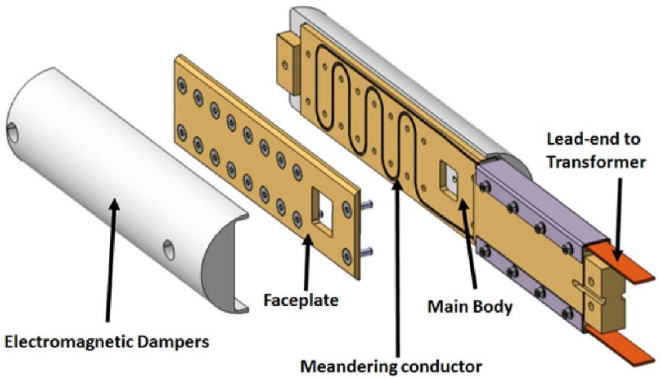

Figure 2. BOX sample assembly, showing the meandering cable in the former, faceplate and aluminium half shell dampers.

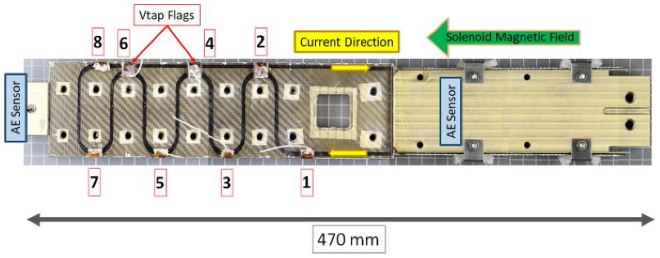

Figure 3. Schematic of instrumentation layout, typical current direction and solenoid field direction. The resulting magnetic force in this configuration pulls sections 1–8 out of the channel. The direction of the current can be reversed to change the orthogonal pulling direction of the magnetic forces.

after reaction heat treatment, impregnation and testing. Once the surface of the cable and main body have been verified after impregnation, the faceplate is screwed unto the main body and hand-tightened to ensure no release during cool down and provide a permanent contact with the main body. Two aluminium half-cylinder shells provide guides for the insertion of the sample into the cryostat well, and minimize the movement of the sample holder under Lorentz forces. Moreover, they act as passive electromagnetic dampers, reducing the inductive coupling with the background solenoid in the case of a sample quench. The cable leads are pre-tinned and then soldered to the Nb–Ti terminals of the transformer secondary coil. Joint resistances of 1 and 2 nΩ were measured for various samples.

BOX samples are designed to expose as much conductor length as possible to the high transverse Lorentz force resulting from the solenoid's magnetic field applied orthogonally to the cable's current direction. Given the free bore of 80 mm in the 11 T facility at the University of Twente, and an empirically determined minimum cable winding radius of 25 mm, up to seven 35 mm long straight sections are exposed to an orthogonal magnetic field.

Depending on the current direction, which itself can be reversed, this results in three or four straight sections being pulled away from the bottom of the channel, while the remaining straight sections are pushed into the channel. The variation of the magnetic background field over the straight sections is less than 1.5 T, with the maximum magnetic field found in the central straight sections. The channel width and depth are adapted to the cable size to minimize the thickness of the pure-epoxy layer at the channel wall, while avoiding insulation damage during the BOX assembly process. The extra channel width typically amounts to 1 mm with respect to the nominal insulated-cable dimensions. Note however, that the nominal dimensions are given for a compacted cable, and that in reality the insulation tends to sufficiently fill the entire channel.

In terms of instrumentation, voltage taps are attached to the cable bends to capture the corresponding onset of a resistive voltage within each straight section, with the aim to identify the sections where a quench occurs as well as to determine the section's critical current. One acoustic sensor is placed at the extremity of the sample to measure acoustic events during current ramping and quenching of sections in the cable. In combination with a 2nd acoustic sensor positioned near the lead-end, it allows to localise the source of the acoustic events. The acoustic sensors' amplification and coupling are reproduced in line with the sensors designed by Marchevsky *et al* [27, 28]. The layout of the instrumentation is shown in figure 3.

2.2. Electromagnetic design

In order to maximize the Lorentz force acting on the straight sections in a specific sample, we estimate the critical current in the BOX cable for different values of the background field. For this purpose, we evaluate the peak magnetic field on the QXF Nb_3Sn quadrupole magnet cable [29, 30] at the strand level and thus the local force. It is a superposition of the variable BOX-sample self-field and the solenoidal background field which is set to a constant value in the direction of the solenoid axis, and the strand self field. Note that the strand self field is added here for consistency, since the available critical-current data equally takes the strand self field into account as it is 'self-field corrected' and is necessary when simulating discretized line currents. The strand and cable properties are shown in table 1.

For relevant levels of the background field, the peak field in the cable is located in a straight section. As an example, figure 4 shows the total magnetic field on strands in a BOX sample at 23 kA in a background magnetic field of 7.5 T. Figure 5 shows the resulting maximum Lorentz-force density in the cable, calculated as the background magnetic field times the estimated critical current, as a function of the background magnetic field. A maximum in Lorentz force is clearly visible at about 7.5 T magnetic background field.

2.3. Forces on sample holder and cable

The shear stress (τ_{zy}) resulting from the Lorentz force (F_y) acting orthogonally to the sample width (thin edge) is estimated using ANSYS Maxwell and its mechanical modules. The finite element geometry is simplified by reducing the number of separate parts and features. The cable itself is considered a homogeneous composite that encompasses averaged properties for the Rutherford cable strands as well as for the epoxy resin and

Table 1. Summary of strand specifications and cable parameters extracted from Ferracin *et al* [29].

Parameters	Unit	
Strand diameter	mm	0, 85
Sub-element diameter	μm	$\leqslant$55
Cu/SC	—	1.2 ± 0.1
RRR	—	>150
Number of strands in cable	—	21
Ic (12 T, 4.2 K), no self-field corr	A	>632

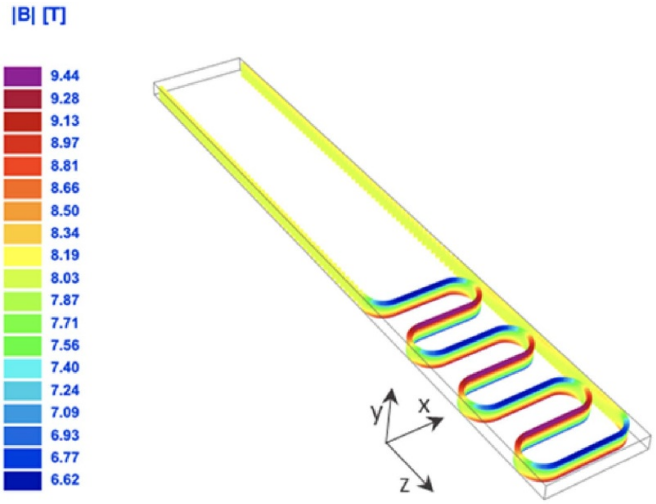

Figure 4. Example of calculated peak magnetic field in a BOX sample, essentially the local vector sum of external magnetic field and cable sample self-field (self-field corrected).

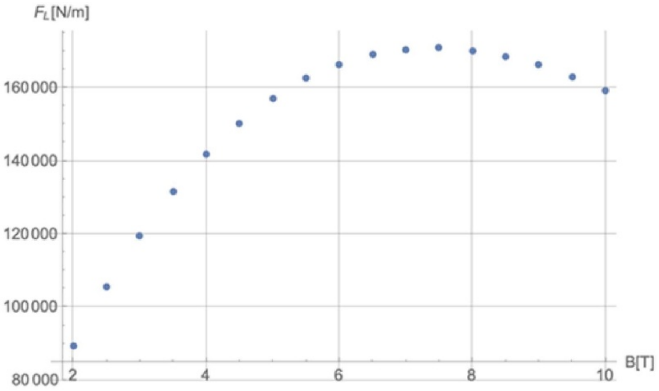

Figure 5. Calculated maximum Lorentz-force density in a BOX wound from a QXF Nb_3Sn cable [29, 30], showing a peak at about 7.5 T background solenoid magnetic field with 23 kA in conductor.

fiberglass. The composite conductor also accounts for anisotropic thermal contraction properties between room temperature and 4.2 K. The main body and faceplate of the BOX samples are modeled using isotropic properties for aluminium bronze.

The bond between the cable and the main body of the holder is modelled using shared nodes. The maximum shear stress is extracted from the surface of the cable in contact with the

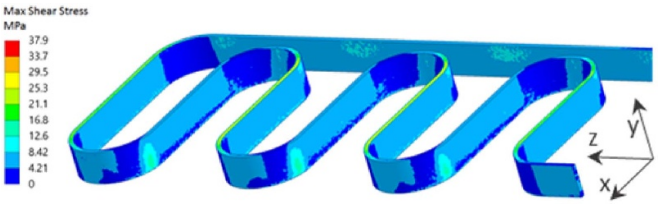

Figure 6. Example of calculated shear stress. In this case of 23 kA cable current in a 7.5 T background field, a maximum shear stress of 38 MPa is observed within the cable composite and a peak shear stress of 10 MPa at the cable/channel interface along the straight sections.

channel of the main body. The cable edge in contact with the faceplate is modelled with a frictional coefficient of 0.2. The faceplate is bonded to the main body using circular contact regions in line with the position and size of the bolts. The boundary conditions for the BOX sample allow the sample to contract at the lead-end where the transformer is connected. The bottom *xz*-face of the main body has restricted displacement in the *y*-direction of the net Lorentz force, which is representative of the contact with the aluminium electromagnetic dampers. The back *xz*-face of the faceplate is free to move.

The FEA reproduces the experimental steps of cooling to 4.2 K and of powering the sample. Here, as an example, a maximum current of 23 kA is present in a background magnetic field of 7.5 T. The resulting magnetic force is approximately 6.1 kN on the 35 mm long straight sections within the high-field region. The magnetic forces extracted from the undeformed ANSYS Maxwell simulation are transferred to the nodes of the ANSYS mechanical model after thermal contraction. The estimated maximum shear stress in the cable/channel interface reaches 10 MPa in the straight sections with peaks of 15 MPa at the transition between straight and bent sections. The average shear stress taken from the central straight section along the width of the cable ranges from 6 to 7 MPa. The maximum shear stresses on the seven straight sections are located either at the bottom edge or at the top edge of the cable depending on the direction of the nodal magnetic forces. A maximum shear stress of 38 MPa is observed within the composite cable structure, see figure 6. Unlike CCT magnets, there is minimal stress accumulation between turns as the cable bends are 22 mm apart.

3. Experimental

3.1. Sample preparation

The BOX samples are prepared at the PSI laboratory using tooling specifically made for inserting the cable into the channel with minimal damage to the insulation. The reaction heat treatment follows the recommended thermal cycle for the specific cable. Prior to impregnation, the cable ends are pre-tinned to minimize infiltration of epoxy resin at the leads due to capillary effects. The eight voltage taps on the cable bends are connected using a silver-loaded glue prior to impregnation.

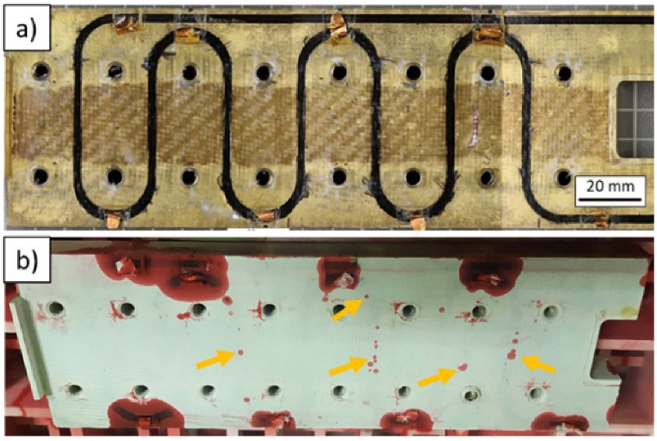

Figure 7. Illustration of the two dyes used for non-destructive examination of the surface of the main body of the BOX containing the meandering cable. Picture (a) shows the optical images of the surface of the sample after removing the faceplate from a tested sample (no surface preparation or polishing was performed). Picture (b) shows the result of the red dye examination, clearly showing defects on the surface along the cable.

The impregnation can be performed for various combinations of atmospheres and impregnation materials. Impregnation is performed in an upright position to ensure that the lead ends remain free from resin. As is common practice in magnets, a fiberglass sheet is placed between the main body of the holder and the faceplate to avoid a layer of pure resin between their surfaces. The surface of the faceplate in contact with the meandering cable and the main body is covered with Teflon tape that allows the faceplate to be removed after impregnation in order to check for initial defects and cracks.

3.2. Post-mortem analysis

A range of post-mortem analyses are performed to assess deterioration as a result of assembly or of powering the sample in a magnetic field at high current. The aim of BOX samples is to identify, characterize and potentially quantify the damage using a number of analytical tools in order to enhance our understanding of the training mechanisms and thus, ultimately, to suggest magnet-relevant solutions.

Non-destructive dye penetrant examination results on BOX samples after testing are shown in figures 7 and 8. The method can be used on already tested and thus damaged samples but also immediately after impregnation to identify pre-existing damage as a result of sample assembly. Two dyes are used: (a) a red dye that provides information on cracks and pores on the surface of the cable; and (b) a fluorescent dye that provides visual information on cracks opened to the surface of the cable and possible propagation of these cracks under the surface of the resin. As the resin is partially transparent, the fluorescent dye can be detected under the surface with a black light as shown in figure 8.

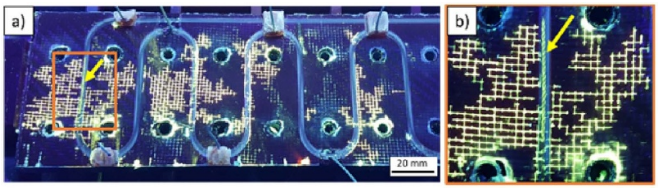

Figure 8. Illustration of the benefits of using a fluorescent dye on BOX-5. Picture (a) shows the dye highlighting cracks along the cable surface as well as poor resin impregnation and wetting with the interlayer fiberglass sheet (possibly as a result of incompatible sizing with the resin). Picture (b) shows the dye having penetrated inside the resin through surface cracks and flowing along the Rutherford cable indicating poor bonding with the cable and resin.

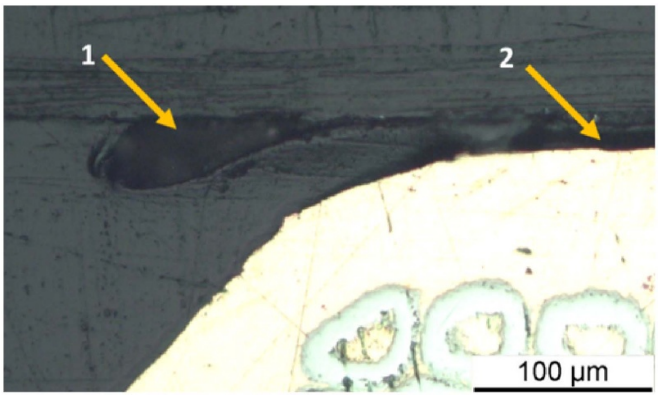

Figure 9. Shows some porosity at location 1 in proximity to the strand but embedded in the composite matrix. Further debonding of the composite matrix from the strand is observed at location 2.

Figure 9 shows an optical image of the cross section of a straight section where magnetic forces are highest. Post-mortem microscopy allows to assess the quality of the impregnation, to identify possible stress concentrators, or to recognize weaknesses in the resin composite that may explain a higher number of quenches in specific sample sections of the sample. The image shows porosity in the composite matrix in proximity to the strand and some debonding occurring at the interface between the strand and the composite in this specific sample.

3.3. Set-up and instrumentation

The BOX samples are tested at the University of Twente in the 11 T, 80 mm bore solenoid facility [31]. The test's magnetic field range chosen depends on the cable's critical current in order to maximize the Lorentz force on the seven straight test sections of the sample.

The cable test current is generated by a superconducting transformer as shown in figure 10. It consists of an 8600-turn primary coil and a 1.5-turn secondary coil with two terminals for connecting the sample. For each 1 A change in primary current a 600 A change in the secondary coil and in the sample is induced. The transformer enables a test current of 50 kA

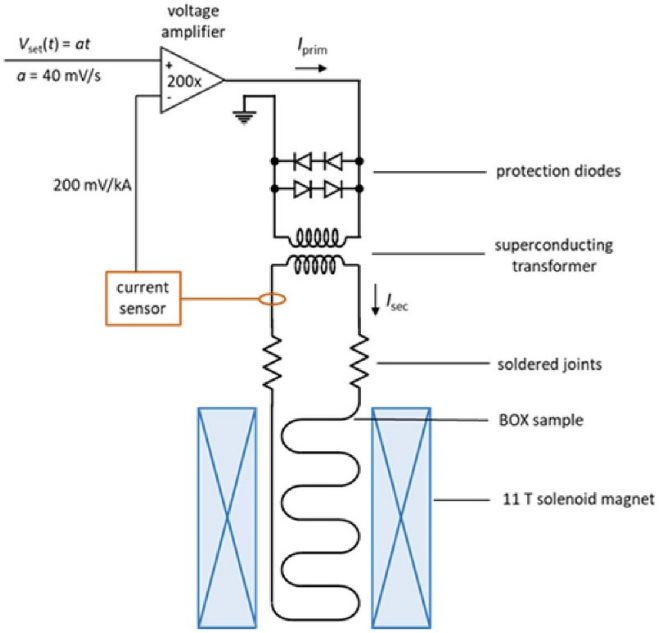

Figure 10. Scheme of the 50 kA superconducting transformer supplying current to the BOX sample inserted in the 11 T magnet through two soldered joint terminals, and its control circuit.

Table 2. Overview of the 1st three BOX sample characteristics.

#	Nb_3Sn conductor	Former	Insulation	Epoxy
BOX 1	RRP 108/127	Alu-bronze	S2 braid + mica layer	Mix 61
BOX 2	RRP 108/127	Alu-bronze	S2 braid	Mix 61
BOX 3	RRP 108/127	Alu-bronze	S2 braid + partial cleaning of sizing	Mix 61

by using $a \pm 50$ A power supply for the primary current (I_{prim}). Use of the superconducting transformer avoids using a high-current supply and warm-cold current leads, drastically reducing the cost of equipment and the consumption of liquid helium.

Due to the 1 and 2 nΩ resistance of the two joints in the secondary circuit for connecting the sample, the secondary current would slowly decay with a time constant of 1000–5000 s. To compensate for this, the transformer is operated in a feedback loop to control the level of the secondary current, as illustrated in figure 10. For the BOX tests, the default ramp rate of the cable current is 200 A s^{-1}. Although the feedback loop compensates for ohmic loss in the joints, it cannot maintain the current at set-point in the case of a quench. Instead, the sample current rapidly decreases when a normal zone develops. Together with the low stored energy in the sample circuit, this means that the sample is self-protected so that active quench detection and protection are not necessary.

As for data acquisition, the sample test current, the voltage drops across all segments in the BOX sample, as well as the acoustic sensor signals, are all recorded with a 100 kHz sampling rate by a multi-channel oscilloscope (Yokogawa DL850EV). For measuring the current, the secondary coil and the BOX sample form a closed circuit within the liquid helium bath. It is therefore not possible to use conventional current sensors that work at room temperature. A current sensor based on a superconducting Rogowski coil circuit was designed specifically to solve this issue. This current sensor is described in detail elsewhere [31]. In addition, the signals are recorded at 1 MHz in a time window of 250 ms before and after a quench event, triggered by a change in current sensed by a hall probe.

4. Typical training results

The main goal of this manuscript is to introduce the BOX experiment itself. The authors have started a systematic campaign to investigate the effect of various material- and layout combinations on the training behaviour of Nb_3Sn cables, as discussed in the section 1. Also the sensitivity and reproducibility of the experiment remains to be confirmed. These results will be reported at a later stage. Nevertheless, to illustrate the performance of the BOX experiment we briefly present here initial data obtained on three Nb_3Sn cable samples of which the main characteristics are presented in table 2.

Identification of the quenching segment is possible by inspecting the timing of the normal-state transitions between the different voltage tap pairs, as shown in figure 11 (bottom) for the 14th quench in BOX sample 3. It is thus possible to gather data on quench localization with respect to current

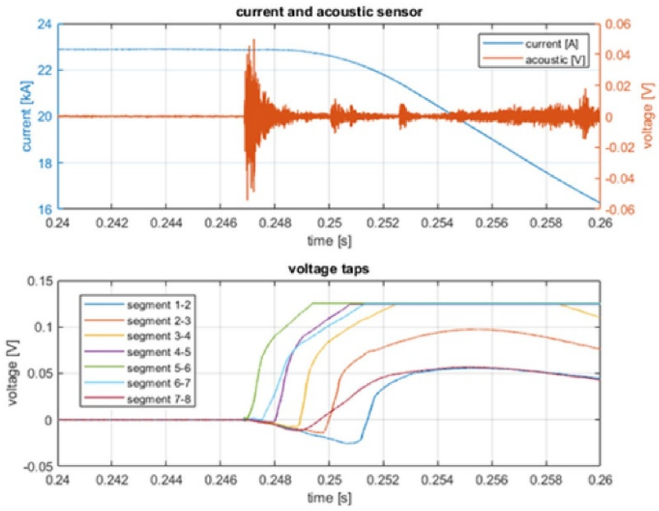

Figure 11. Recorded acoustic and current traces during training quench #14 in sample BOX 3 (top); and corresponding sample voltages (bottom).

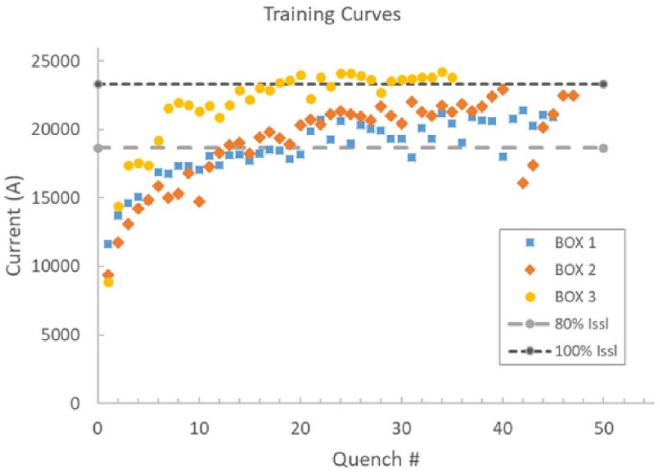

Figure 12. Training curves of the 1st 3 Nb_3Sn BOX samples measured, convincingly demonstrating characteristic 'magnet' training behaviour.

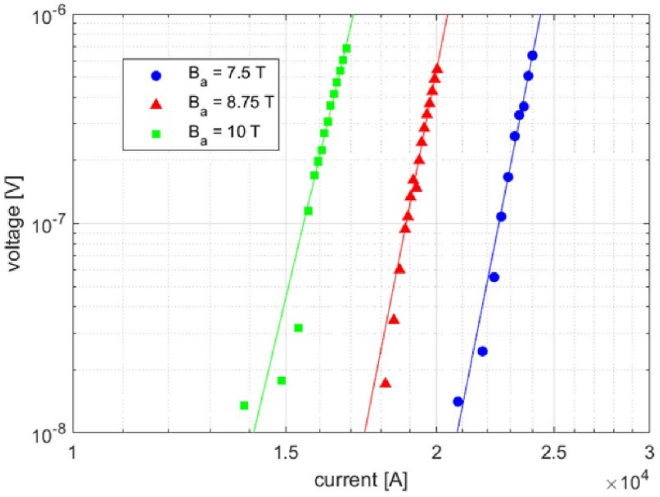

Figure 13. Example of *V–I* measurements performed on BOX 6 at 7.5 T, 8.75 T and 10 T.

direction and local Lorentz force direction (pulling sequential cable sections in or out of channel).

As a further illustration, figure 11 (top) shows the recorded 1 MHz data for the same quench. The current was increased at a rate of 200 A s^{-1} to a maximum of 22.9 kA. A sudden increase of voltage and decrease of current occurs at $t = 250$ ms, triggering the oscilloscope. The voltage 1st rises in segments 5 and 6 at $t = 247$ ms, shortly followed by its neighbouring segments 4 to 5 and 6 to 7, a pattern typical for normal zone propagation. At $t = 251$ ms, the normal zone reached the most distant segments 1 and 2. The segments that have not yet been reached by the normal zone show a negative voltage. This can be understood as an inductive voltage caused by the rapid decrease in current.

The acoustic sensor recorded an event at $t = 247$ ms that occurred simultaneously with the 1st rise in voltage. Further analysis is underway to localize the source of the acoustic events (to confirm that they indeed correlate with the position of normal zone initiation), and to study their specific 'fingerprint' (to seek for possible correlations with features observed in the 'post-mortem' analysis).

The training curves of the 1st three illustrative samples are compared in figure 12. The uncertainty on the quench current is estimated to be 1%. The samples exhibit a qualitatively similar training behaviour as full-scale magnets, albeit plateauing closer to the cables' critical current [14].

V–I measurements were performed on an additional Nb_3Sn sample (BOX 6) as the sample reached and surpassed the predicted critical current of 23.3 kA. This sample was impregnated using paraffin wax unlike previous BOX samples using epoxy resins. In this sample, the only quenching segment was segments 4 and 5 in the high-field region, therefore *V–I* measurements were performed on this segment alone. As shown in figure 13, measurements were taken at 7.5 T, 8.75 T and 10 T background field over the segments 4 and 5 where the I_c is the lowest.

5. Discussion

The initial BOX samples presented here to demonstrate the characteristic results that can be achieved, have followed an assembly process mimicking the construction of CCT magnets. The samples exhibited similar training behaviour as found in full-scale magnets, albeit plateauing at currents close or sometimes even just above the short sample critical current following the 10 μV m^{-1} criterion. The samples start training at or above 40% of the critical current and reach 80% between 6 and 17 quenches, depending on the improvements made during fabrication. Quenches are detected in varying amounts in different sections and are not all necessarily in the peak field region of the central segments.

Remarkably, the BOX 3, where improvements were made for bonding, reached 80% of the expected critical current in six quenches and plateaued at or even slightly above the estimated

critical current of 23.3 kA assuming 5% cable degradation with respect to the virgin wire critical current. To ensure reproducibility of the result, additional samples are to be fabricated in the future.

These observations illustrate how the BOX experiment indeed appears to constitute an efficient test bench for rapid assessment of design improvements from one sample to another. Furthermore, the ability to produce slightly varying samples allows for a quick and efficient screening of promising fabrication methods and materials that warrant further reproducible and statistically relevant sample quantities. Therefore, it is envisaged that these improvements are trialed using BOX samples prior to implementing them into more costly demonstration magnets with even more representative operational conditions.

The ability to reach currents very close to the critical current may also indicate that forces do not introduce as much damage or instabilities as in full-scale magnets. This may be explained by the larger spacing between the conductor turns, which reduces the interaction between neighbouring channels and the resulting stress/strain interaction, by the ideal flat structure of the BOX geometry, by forces acting orthogonal to the channels, and by the improved control of the assembly process due to the smaller size of the BOX samples. In order to further reproduce high-field magnet behaviour, it may be feasible to wind two cables in parallel in one channel owed to the flexibility of the solenoid to supply up to 50 kA to two cables. This method could double the forces pulling the cables out of the channel. Furthermore, there is room for alterations to the BOX design by adding spot heaters to trigger quenches and to promote additional stress conditions by implementing *in situ* compressive stresses on the broad face of the cable during powering as is already performed at the facility [32]. Nonetheless, the BOX acoustic and voltage tap signals are comparable to those recorded in full-scale magnets, but this time in response to forces that are more easily characterised and controlled.

Another key advantage of the BOX experiment—besides its cost-effectiveness and high sample throughput—is the relatively simple distribution of magnetic forces acting on the conductor in the background field of the solenoid. The uniaxial nature of the force simplifies the determination of the critical von Mises and shear stresses that act on the cable and interfaces. Using the analogy of uniaxial tensile test specimens, the BOX samples can thus provide a means for evaluating material properties as well as contact surface properties, to calibrate finite element simulations and to help to predict conductor behaviour in more complex magnet structures.

6. Conclusion

The BOX experiment constitutes a relatively low-cost test bench for studying the behaviour of interfaces between cable, epoxy resin, insulation material and formers used in magnet research and development. The experiment exposes a number of meandering segments of a cable to an orthogonal magnetic field, thus generating magnet-relevant Lorentz shear stress levels of the order of 10 MPa or higher. This level is often used as a limit for the mechanical stability of interfaces in accelerator magnets [33].

The sample is powered using a 50 kA superconducting transformer and instrumented with multiple voltage taps and acoustic sensors, allowing to accurately monitor and locate training quenches in a way similar to representative magnets, but under precisely controlled conditions. The design of the BOX experiment allows for a wide use of material examining methods, which are needed for understanding training in different systems.

The ultimate goal of using this test bench is to increase the reliability of superconducting accelerator magnets by relatively rapid testing and selection of solutions, and by improving our understanding of potential training issues and related operating margins.

Data availability statement

The data that support the findings of this study are available upon reasonable request from the authors.

Acknowledgments

The authors are thankful to Arjan Verweij from CERN for his feedback and suggestions for the meandering cable and optimisation of the design of the BOX samples.

ORCID iDs

Michael Daly https://orcid.org/0000-0002-7584-2996
Bernard Auchmann https://orcid.org/0000-0002-3407-8864
Anna Kario https://orcid.org/0000-0002-7241-3707
Herman Ten Kate https://orcid.org/0000-0001-5597-3190

References

[1] Stoynev S *et al* 2019 Analysis of Nb_3Sn accelerator magnet training *IEEE Trans. Appl. Supercond.* **29** 7–12
[2] Devred A 2002 Insulation systems for Nb_3Sn accelerator magnet coils manufactured by the wind and react technique *IEEE Trans. Appl. Supercond.* **12** 1232–7
[3] Dotsenko V I *et al* 1991 Effect of epoxy debonding and cracking on stability of superconducting composites *Cryogenics* **31** 906–12
[4] Auchmann B, Brouwer L, Caspi S, Gao J, Montenero G, Negrazus M, Rolando G and Sanfilippo S 2018 Electromechanical design of a 16 T CCT twin-aperture dipole for FCC *IEEE Trans. Appl. Supercond.* **28** 7–11
[5] Montenero G, Auchmann B, Brouwer L, Calzolaio C, Caspi S, Rolando G and Sanfilippo S 2018 Mechanical structure for the PSI canted-cosine-theta (CCT) magnet program *IEEE Trans. Appl. Supercond.* **28** 1–5
[6] Caspi S *et al* 2014 Canted-cosine-theta magnet (CCT)—a concept for high field accelerator magnets *IEEE Trans. Appl. Supercond.* **24** 1–4
[7] Brouwer. L 2016 UC Berkeley electronic theses and dissertations *DNA Mediat. Assem. Protein Heterodimers Membr. Surfaces* p 67 (available at: https://escholarship.org/uc/item/98384265)

[8] Novitski I 2021 SMCT magnet status and next steps *US-MDP Collab. Meet. 2021* pp 1–16 (available at: https://conferences.lbl.gov/event/547)

[9] Novitski I *et al High-field Nb_3Sn Cos-theta Dipole with Stress Management* pp 15–18

[10] Felice H *et al* 2010 Test results of TQS03: a LARP shell-based Nb_3Sn quadrupole using 108/127 conductor *J. Phys.: Conf. Ser.* **234** 032010

[11] Bajko M *et al* 1998 Training study on superconducting coils of the LHC sextupole corrector magnet *LHC Project Report 236; Presented at EPAC 98, Stockholm, Sweden*

[12] Vallone G and Ferracin P 2017 Modeling coil-pole debonding in Nb_3Sn superconducting magnets for particle accelerators *IEEE Trans. Appl. Supercond.* **27** 1–11

[13] Prestemon S 2018 Status update from LBNL MDP–FCC–EuroCirCol meeting *History of CCT Dipole Tests at LBNL*

[14] Prestemon S 2019 CCT magnet development: results and next steps *International Meeting on High Field Accelerator Magnet Research and Review of Recent US MDP Progress and Plans (4–5 December 2019)* (Gaithersburg, MD: Gaithersburg Marriott Washingtonian Center)

[15] Maeda H *et al* 1982 Heat generation from epoxy cracks and bond failures *Cryogenics* **22** 473–6

[16] Fujita H *et al* 1985 Experimental and theoretical investigation of mechanical disturbances in epoxy-impregnated superconducting coils. 4. Prequench cracks and frictional motion *Cryogenics* **25** 323–6

[17] Granieri P P, Lorin C and Todesco E 2011 Slip-stick mechanism in training the superconducting magnets in the large hadron collider *IEEE Trans. Appl. Supercond.* **21** 3555–60

[18] Maressa P, Anodio L, Bernasconi A, Demir A G and Previtali B 2014 Effect of surface texture on the adhesion performance of laser treated Ti_6Al_4V alloy *J. Adhes.* **91** 518–37

[19] Davis G D 1993 Contamination of surfaces: origin, detection and effect on adhesion *Surf. Interface Anal.* **20** 368–72

[20] Yin S, Arbelaez D, Swanson J and Shen T 2019 Epoxy resins for vacuum impregnating superconducting magnets: a review and tests of key properties *IEEE Trans. Appl. Supercond.* **29** 1–5

[21] Yin S, Swanson J and Shen T 2020 Design of a high toughness epoxy for superconducting magnets and its key properties *IEEE Trans. Appl. Supercond.* **30** 1–5

[22] Ambrosio G *et al* 2021 Lessons learned from the prototypes of the MQXFA low-beta quadrupoles for HL-LHC and status of production in the US *IEEE Trans. Appl. Supercond.* **31** 8–13

[23] Brem A *et al* 2021 Elasticity, plasticity and fracture toughness at ambient and cryogenic temperatures of epoxy systems used for the impregnation of high-field superconducting magnets *Cryogenics* **115** 1–11

[24] Haubenreich P N *et al* 1970 Experimental and theoretical studies of filamentary superconducting composites *J. Phys. D: Appl. Phys.* **3** 1517–85

[25] Roy S S, Potluri P, Canfer S and Ellwood G 2018 Braiding ultrathin layer for insulation of superconducting Rutherford cables *J. Ind. Text* **48** 827–47

[26] Barzi E *et al* 2020 Heat diffusion in high-Cp Nb_3Sn composite superconducting wires **4** 1–13

[27] Marchevsky M, Sabbi G, Bajas H and Gourlay S 2015 Acoustic emission during quench training of superconducting accelerator magnets *Cryogenics* **69** 50–57

[28] Marchevsky M, Arbelaez D and Prestemon S 2020 Structural diagnostics of superconducting magnets using diffuse field ultrasound *IEEE Trans. Appl. Supercond.* **30** 8–11

[29] Ferracin P *et al* 2019 The HL-LHC low-β quadrupole magnet MQXF: from short models to long prototypes *IEEE Trans. Appl. Supercond.* **29** 2–9

[30] Ferracin P *et al* 2016 Development of MQXF, the Nb_3Sn low-β quadrupole for the HiLumi LHC *24th Int. Conf. on Magnet Technology (MT24)* vol 1 (https://doi.org/10.1109/TASC.2015.2510508)

[31] Weijers H W *et al* 1994 Improved superconducting direct current meter for 25–50 kA *Advances in Cryogenic Engineering* ed P Kittel (Boston, MA: Springer US) pp 1147–52

[32] van de Camp W 2012 Critical current versus transverse stress and thermal stability of RRP Nb_3Sn Rutherford cable Master Thesis (available at: http://purl.utwente.nl/essays/62400)

[33] Ortwein R, Blocki J, Wachal P, Kirby G and van Nugteren J 2020 FEM modeling of multilayer canted cosine theta (CCT) magnets with orthotropic material properties *Cryogenics* **107** 103041